

Regular Paper

CBR-ACE: Counting Human Exercise using Wi-Fi Beamforming Reports

SORACHI KATO^{1,a)} TOMOKI MURAKAMI² TAKUYA FUJIHASHI¹ TAKASHI WATANABE¹
SHUNSUKE SARUWATARI¹

Received: July 7, 2021, Accepted: September 9, 2021

Abstract: As people spend more time indoors owing to the COVID-19 global pandemic, the automatic detection of indoor human activity has increasingly become of interest to researchers and consumers. Conventional Wi-Fi Channel State Information (CSI)-based detection provides adequate accuracy; however, they have a deployment constraint owing to specific hardware and software for full CSI acquisition. This study exploits the Compressed Beamforming Report (CBR), which is a default form of CSI in IEEE 802.11ac and 11ax, to address the constraint in Wi-Fi CSI-based methods. The CBRs are shared among most IEEE 802.11ac compliant devices and are easily obtained with outer sniffers. Our CBR-based Activity Count Estimator (CBR-ACE) is a novel wireless sensing system using CBRs. The CBR-ACE provides a Raspberry Pi-based tool to easily deploy a new wireless sensing system into existing networks, and utilizes the CBR irregularity for automatic detection. From experiments in real-dwelling environments, the proposed CBR-ACE achieves average estimation errors of 0.97 in the best case.

Keywords: wireless LAN, remote sensing, channel state information, activity recognition

1. Introduction

Owing to the COVID-19 pandemic, the number of people working remotely from their homes and attending lectures has increased significantly to limit the spread of the infection. According to Ref. [1], approximately 35% of the targeted samples in the US reported that they recently switched to working from home. However, the problem of inactivity is rising as people stay-at-home for a long period. Owing to the physical distancing restrictions and recommendation for self-isolation at home, many people are failing to continue with their regular outdoor exercises; instead, they operate indoor exercise, e.g., repetitive exercises, such as twisting or push-ups, for improving cognitive and emotional well-being. Therefore, systems that automatically detect and continuously measure these indoor exercises will make it easier for people to manage their activeness and stay healthy.

Some studies have demonstrated an automatic tracking of human activity. **Table 1** lists the pros and cons of the existing studies on human activity sensing. The typical systems utilize visual- or sensor-based sensing methods. These methods have had a significant success in human activity recognition [2] and wild life tracking [3]. However, the visual-based methods fundamentally require Line-of-Sight (LOS) and bright environments without any obstacles. In addition, the visual-based methods can cause serious privacy issues. The sensor-based methods are relatively cheap and easy to deploy. With the recent development

Table 1 Comparison of human activity sensing methods.

Sensing Method		Pros	Cons
Visual		Rich information	Depends on lighting condition, Potential privacy issue
Sensor		Low cost, Easy deployment	Depends on the sensor placement, Battery life
Wireless	Custom Hardware	UWB	Giga-hertz bandwidth, Multipath robustness
	COTS Devices	RSSI	Easy to obtain
		Full CSI	Works with 802.11n/ac standards, Fine-grained
		CBR	Works with 802.11ac/ax standards, Higher accessibility than full CSI
			Coarse-grained
			Requires specific NICs to obtain
			Insufficient discussion about proper processing for sensing

of neural networks, sensor-based activity recognition with fairly high accuracy has been achieved [4], [5]. However, their accuracy depends on where and how the sensors are set on the environment. Furthermore, a significant problem that sensor devices experience is the battery life.

In recent years, wireless sensing methods have been extensively studied as a new sensing method. Wireless sensing can perform high-precision sensing while solving the aforementioned issues of the existing sensing methods. Although some studies utilize wireless signals from a high frequency band, such as the Ultra Wide Band (UWB) [6], most of these wireless sensing methods are designed for commercial off-the-shelf (COTS) wireless devices. Particularly, they exploit Channel State Information (CSI), which is defined after the IEEE 802.11n standards as a method to indicate the channel dynamics between the wireless devices, for sensing in non-LOS (NLOS) environments and over long distances. For example, they realized human localization [7], activity recognition [8], and fall detection [9] by coping with the channel dynamics for sensing. Additionally, a recent work proposed Wi-COVID for COVID-19 patient monitoring [10]. Although there are sensing methods using RSSI [11], [12], RSSI

¹ Graduate School of Information Science and Technology, Osaka University, Suita, Osaka 565-0871, Japan

² Access Network Service Systems Laboratory, NTT Corporation, Yokosuka, Kanagawa 239-0847, Japan

^{a)} kato.sorachi@ist.osaka-u.ac.jp

that can be obtained by COTS devices is coarse-grained and only one value can be obtained from a single packet, so the method using CSI can provide more detailed sensing.

However, there are large gaps between the assumed COTS wireless devices in the existing CSI-based sensing studies and the recent COTS wireless devices. The COTS wireless devices in most of these existing methods need to equip a certain type of Network Interface Card (NIC) such as Intel 5300, which follows the IEEE 802.11n standard, to obtain full CSI for sensing. However, the COTS wireless devices are equipped with a variety of NICs and most of them are compliant with the subsequent standards, such as IEEE 802.11ac and 11ax. In both IEEE 802.11ac and 11ax, the full CSI is transformed into eigen space and the space is quantized into binary to reduce communication overhead. Although the COTS wireless devices can reconstruct the compressed eigen space, which refers to Compressed Beamforming Reports (CBRs), by decoding the received binary, its nature totally differs from the full CSI.

To fill the gaps, the next generation of wireless sensing systems, using the COTS wireless devices should realize the following functions:

- (1) A tool that can reconstruct the CBRs from the binary without requiring a dedicated device for decoding and NICs on the COTS wireless devices.
- (2) A sensing method that can recognize human activity and exercise only using the CBRs.

Therefore, we propose a novel wireless sensing system, namely, CBR-based Activity Count Estimator (CBR-ACE). CBR-ACE consists of two methods to realize the aforementioned functions. CBR-ACE includes: 1) WiPiCap and 2) ACE. WiPiCap realizes Raspberry Pi-based packet sniffer and binary decoding to collect the CBRs without the limitation of the NICs on the COTS wireless devices. WiPiCap not only acquires data, but also generates time series data from the decoded information. We make WiPiCap open-source and publicly available. ACE is a signal processing-based recognition of human exercise, i.e., the number of repetitive exercises, using the time-series of the CBRs.

The contributions of this paper can be summarized as follows:

- (1) To the best of our knowledge, CBR-ACE is the first wireless sensing system to estimate human activity counts using the CBRs.
- (2) WiPiCap is the first tool to process packet sniffing, binary decoding, and constructing time-series data for CBRs.
- (3) ACE recognizes human exercise using a well-known signal processing, and thus, a low computational requirement for the recognition compared with machine and deep learning-based methods.
- (4) CBR-ACE achieves an estimation error of 1.73 on average, and 0.97 in the best case.

2. Related Works

RF-based Activity Recognition. In RF propagation, radio irregularity rises to a higher level in the presence of human activity (briefly shown in **Fig. 1**). For the radar-based system, some techniques such as Doppler Shift [13] and UWB [14] have been designed to extract even small movements. In recent years, a fre-

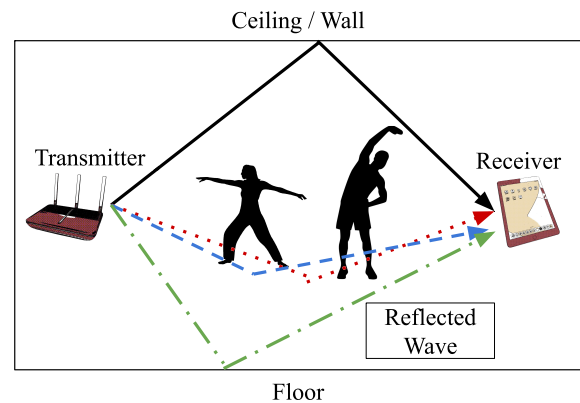


Fig. 1 General model of wireless sensing system in the presence of human activity.

quency modulated continuous wave (FMCW) radar was adopted in the research field [15]. However, they required special hardware with high frequency.

To build wireless sensing systems with more familiar devices with a low cost, Wi-Fi based passive systems are proposed. They utilize full CSI in IEEE 802.11n for the systems. The full CSI demonstrates how the input signal is impaired by the channel to the wireless device in the MIMO communication system. The main idea of these studies is that channel responses are distorted by the presence of humans or the humans activity and the correlation between the activity and the full CSI is unique in both the time- and frequency-domains.

In Ref. [16], full CSI amplitudes are fed to a combination of three types of deep neural networks (DNNs) for activity recognition. The recognition realized human and receiver locations with an average accuracy of 97%. The CSI based human Activity Recognition and Monitoring system (CARM) [17] models the correlation between human movements and speed, transfers CSI amplitude variation into speed information, and recognizes a given activity using the Hidden Markov Model.

CBR-based Activity Recognition. Although the full CSI-based sensing exhibit a high accuracy, they inhibit the movement from the research stage to the commercial development stage owing to the requirement of specific hardware and software [18], [19]. The most recent COTS devices are IEEE 802.11ac/ax compliant, and thus support CBRs instead of the full CSI. CBRs are shared between the transmitter and receiver without encryption, making them easy to obtain from an external sniffer [20]. It is obvious that the CBRs are essential for the building of the passive sensing system based on IEEE 802.11ac/ax standards; however, there are several challenges in the research field as follows:

- (1) Until now, there is no finding on CBRs to be used as an information source for human activity recognition.
- (2) Although we found that the raw CBRs cause low accuracy from prior experiments, there is no study on how to obtain effective CBRs from the raw CBRs for the recognition.
- (3) Because the radio irregularity differs among the subcarriers, an adequate subcarrier selection may impact the recognition accuracy.

So far, there are only a few research studies making efforts towards building CBR-based sensing. Reference [20] estimates

the number of walking people through walls using CBRs. In Ref. [21], the system is developed to localize a person outdoors. Besides, in our recent work [22], we proposed a direct CBR-to-image conversion system with the power of Generative Adversarial Networks (GANs). The research studies presented above realized sensing systems based on CBRs, achieving reasonable accuracy; however, they all depend on the ability of machine and deep learning. This means that they need an enough number of training data sets for sensing.

3. Compressed Beamforming Reports (CBRs) in IEEE 802.11ac/ax

In IEEE 802.11n and its successors, Multiple Input Multiple Output (MIMO) is an essential technique to gain the capacity of a radio link. Specifically, MIMO can increase the diversity, array, and multiplexing gains with the reduction on the co-channel interference. In an ordinary indoor environment, the transmitted signals are reflected and attenuated owing to obstacles in indoor spaces. The environment is also referred to as the “multipath environment”. The received signal in the multipath environments is represented as the superposition of multiple transmitted waveforms traveling along the different paths before arriving at the receiver. The main mission of the receiver is to reconstruct original signals, which are transmitted from each transmission antenna, from the received signal. IEEE 802.11n solves this problem using full CSI to estimate a model of the multipath environment. Once the receiver acquires the full CSIs, the transmitted signal can be estimated using post-equalization including Zero-Forcing (ZF) and minimum mean square error (MMSE) equalizations [23].

Although a diversity of the channel dynamics exists in the measured CSI, the ZF and MMSE equalizations provide coarse estimation about the transmitted signal. To solve the problem in the post equalizations, recent works take precoding for the transmission signals. The typical solution is Eigenspace Spatial Division Multiplication (E-SDM). In E-SDM, a mathematical process referred to as Singular Value Decomposition (SVD) is applied to the full CSI, and the resulting right singular matrix is multiplied by the transmitted signal in advance to form an orthogonal beam space, so that the receiver can receive signals from each transmission antenna without interference.

We assume one transmitter and one receiver communicate on the same and single wireless channel. The number of antenna for the transmitter and receiver is set as M and N , respectively. In this case, the received signal can be modeled as:

$$\mathbf{y} = \mathbf{H}\mathbf{x} + \mathbf{n}, \quad (1)$$

where $\mathbf{x} \in \mathbb{C}^{1 \times M}$ and $\mathbf{y} \in \mathbb{C}^{1 \times N}$ are the signal vectors transmitted by the transmitter and received by the receiver, respectively. Additionally, $\mathbf{n} \in \mathbb{C}^{1 \times N}$ is the Additive White Gaussian Noise (AWGN) vector and $\mathbf{H} \in \mathbb{C}^{N \times M}$ is the channel information matrix, i.e., full CSI. The full CSI can be decomposed by SVD as shown in Eq. (2):

$$\mathbf{H} = \mathbf{U}\mathbf{\Sigma}\mathbf{V}^H, \quad (2)$$

where \mathbf{U} and \mathbf{V} are the left and right singular matrices, which are

complex and unitary matrices, and $\mathbf{\Sigma}$ is a diagonal matrix whose i th diagonal element is the singular value of the full CSI. The singular values are associated with the substream amplitude gains. Further, \mathbf{V}^H indicates the Hermitian transpose of the matrix \mathbf{V} . Equation (2) is then substituted into Eq. (1) as:

$$\mathbf{y} = \mathbf{U}\mathbf{\Sigma}\mathbf{V}^H\mathbf{x} + \mathbf{n}. \quad (3)$$

In E-SDM, the transmitter precodes the transmission signal \mathbf{x} by multiplying the right singular matrix \mathbf{V} so that the precoded signal $\hat{\mathbf{x}}$ is spatially orthogonal and interference-free. In this case, the received signal is expressed as:

$$\begin{aligned} \mathbf{y} &= \mathbf{H}\hat{\mathbf{x}} + \mathbf{n} \\ &= \mathbf{U}\mathbf{\Sigma}\mathbf{V}^H\mathbf{V}\mathbf{x} + \mathbf{n} \\ &= \mathbf{U}\mathbf{\Sigma}\mathbf{x} + \mathbf{n}. \end{aligned} \quad (4)$$

Finally, the left singular matrix \mathbf{U}^H is multiplied to the received signal to obtain the reconstructed signal of $\mathbf{\Sigma}\mathbf{x} + \mathbf{n}$. It indicates that the orthogonal transmission with the substream gains corresponding to the singular values can be made by the eigenbeams. For the orthogonal transmission, the transmitter and receiver need to share the right singular matrix \mathbf{V} for precoding. Hence, the transmitter transmits $(\min(M, N))^2$ complex elements to the receiver as the metadata. The large communication overhead may cause rate and power losses in wireless communications.

The recent IEEE 802.11ac/ax compliant COTS Access Points (APs) and wireless devices introduce Givens Rotation and quantization for overhead reduction [24]. Let M be equal or greater than N , and $\hat{\mathbf{V}}$ be the part of up to the m th row and n th column of matrix \mathbf{V}^H . Specifically, the matrix $\hat{\mathbf{V}}$ can be decomposed as follows:

$$\hat{\mathbf{V}} = \left[\prod_{i=1}^{\min(N, M-1)} \left[D_i \prod_{l=i+1}^M G_{li}^T(\Psi_{li}) \right] \right] \tilde{\mathbf{I}}_{M \times N}, \quad (5)$$

where D_i and G_{li} are derived as follows:

$$D_i = \begin{bmatrix} I_{i-1} & 0 & \dots & \dots & 0 \\ 0 & e^{j\phi_{i,i}} & 0 & \dots & 0 \\ \vdots & 0 & \ddots & 0 & 0 \\ \vdots & \vdots & 0 & e^{j\phi_{M-i,i}} & 0 \\ 0 & 0 & 0 & 0 & 1 \end{bmatrix},$$

$$G_{li}(\psi) = \begin{bmatrix} I_{i-1} & 0 & 0 & 0 & 0 \\ 0 & \cos(\psi) & 0 & \sin(\psi) & 0 \\ 0 & 0 & I_{l-i-1} & 0 & 0 \\ 0 & -\sin(\psi) & 0 & \cos(\psi) & 0 \\ 0 & 0 & 0 & 0 & I_{M-l} \end{bmatrix}.$$

Here, G is Givens rotation matrix in rows l and i . Each I_k is an $k \times k$ identity matrix and $\tilde{\mathbf{I}}_{M \times N}$ is an identity matrix padded with zeros to fill the additional rows/columns at $M \neq N$. Hence any basis matrix is represented with angle variables of $\phi_{k,l}$ and $\psi_{k,l}$.

We explain the parameterization procedure with a 4×2 matrix $\hat{\mathbf{V}}$ assuming MIMO communication with 4 receiving antennas and 2 transmitting antennas:

$$\hat{\mathbf{V}} = \begin{bmatrix} v_{11}^{(0)} & v_{12}^{(0)} \\ v_{21}^{(0)} & v_{22}^{(0)} \\ v_{31}^{(0)} & v_{32}^{(0)} \\ v_{41}^{(0)} & v_{42}^{(0)} \end{bmatrix},$$

where $v_{ij}^{(l)} \in \mathbb{C}$ is the element in the right singular matrix after the l th Givens rotation. We first make the elements in the bottom row to have real and absolute-valued elements as follows:

$$\hat{\mathbf{V}} = \begin{bmatrix} v_{11}^{(0)} & v_{12}^{(0)} \\ v_{21}^{(0)} & v_{22}^{(0)} \\ v_{31}^{(0)} & v_{32}^{(0)} \\ v_{41}^{(0)} & v_{42}^{(0)} \end{bmatrix} \begin{bmatrix} \frac{v_{41}^{(0)}}{|v_{41}^{(0)}|} & 0 \\ 0 & \frac{v_{42}^{(0)}}{|v_{42}^{(0)}|} \end{bmatrix}^H = \begin{bmatrix} v_{11}^{(1)} & v_{12}^{(1)} \\ v_{21}^{(1)} & v_{22}^{(1)} \\ v_{31}^{(1)} & v_{32}^{(1)} \\ |v_{41}^{(0)}| & |v_{42}^{(0)}| \end{bmatrix},$$

Next, we multiply D_1 to make the elements in the first column be real numbers as follows:

$$D_1 = \begin{bmatrix} \exp(j\phi_{11}) & 0 & 0 & 0 \\ 0 & \exp(j\phi_{21}) & 0 & 0 \\ 0 & 0 & \exp(j\phi_{31}) & 0 \\ 0 & 0 & 0 & 1 \end{bmatrix},$$

$$\exp(j\phi_{11}) = \frac{v_{11}^{(1)}}{|v_{11}^{(1)}|}, \quad \exp(j\phi_{21}) = \frac{v_{21}^{(1)}}{|v_{21}^{(1)}|}, \quad \exp(j\phi_{31}) = \frac{v_{31}^{(1)}}{|v_{31}^{(1)}|},$$

$$D_1^H \begin{bmatrix} v_{11}^{(1)} & v_{12}^{(1)} \\ v_{21}^{(1)} & v_{22}^{(1)} \\ v_{31}^{(1)} & v_{32}^{(1)} \\ |v_{41}^{(0)}| & |v_{42}^{(0)}| \end{bmatrix} = \begin{bmatrix} v_{11}^{(2)} & v_{12}^{(2)} \\ v_{21}^{(2)} & v_{22}^{(2)} \\ v_{31}^{(2)} & v_{32}^{(2)} \\ v_{41}^{(2)} & v_{42}^{(2)} \end{bmatrix} = \begin{bmatrix} |v_{11}^{(1)}| & v_{12}^{(2)} \\ |v_{21}^{(1)}| & v_{22}^{(2)} \\ |v_{31}^{(1)}| & v_{32}^{(2)} \\ |v_{41}^{(0)}| & |v_{42}^{(0)}| \end{bmatrix}.$$

For the first and second rows of the matrix, we define the Givens rotation matrix G_{21} as follows:

$$G_{21} = \begin{bmatrix} \cos \psi_{21} & \sin \psi_{21} & 0 & 0 \\ -\sin \psi_{21} & \cos \psi_{21} & 0 & 0 \\ 0 & 0 & 1 & 0 \\ 0 & 0 & 0 & 1 \end{bmatrix},$$

$$\cos \psi_{21} = \frac{|v_{11}^{(1)}|}{\sqrt{|v_{11}^{(1)}|^2 + |v_{21}^{(1)}|^2}}, \quad \sin \psi_{21} = \frac{|v_{21}^{(1)}|}{\sqrt{|v_{11}^{(1)}|^2 + |v_{21}^{(1)}|^2}},$$

$$G_{21} D_1^H \begin{bmatrix} v_{11}^{(1)} & v_{12}^{(1)} \\ v_{21}^{(1)} & v_{22}^{(1)} \\ v_{31}^{(1)} & v_{32}^{(1)} \\ |v_{41}^{(0)}| & |v_{42}^{(0)}| \end{bmatrix} = \begin{bmatrix} \sqrt{|v_{11}^{(1)}|^2 + |v_{21}^{(1)}|^2} & v_{12}^{(3)} \\ 0 & v_{22}^{(3)} \\ |v_{31}^{(1)}| & v_{32}^{(2)} \\ |v_{41}^{(0)}| & |v_{42}^{(0)}| \end{bmatrix}.$$

Similarly, we define G_{31} and G_{41} as follows:

$$G_{31} = \begin{bmatrix} \cos \psi_{31} & 0 & \sin \psi_{31} & 0 \\ 0 & 1 & 0 & 0 \\ -\sin \psi_{31} & 0 & \cos \psi_{31} & 0 \\ 0 & 0 & 0 & 1 \end{bmatrix},$$

$$\cos \psi_{31} = \frac{\sqrt{|v_{11}^{(1)}|^2 + |v_{21}^{(1)}|^2}}{\sqrt{|v_{11}^{(1)}|^2 + |v_{21}^{(1)}|^2 + |v_{31}^{(1)}|^2}},$$

$$\sin \psi_{31} = \frac{|v_{31}^{(1)}|}{\sqrt{|v_{11}^{(1)}|^2 + |v_{21}^{(1)}|^2 + |v_{31}^{(1)}|^2}},$$

$$G_{41} = \begin{bmatrix} \cos \psi_{41} & 0 & 0 & \sin \psi_{41} \\ 0 & 1 & 0 & 0 \\ 0 & 0 & 1 & 0 \\ -\sin \psi_{41} & 0 & 0 & \cos \psi_{41} \end{bmatrix},$$

$$\cos \psi_{41} = \sqrt{|v_{11}^{(1)}|^2 + |v_{21}^{(1)}|^2 + |v_{31}^{(1)}|^2}, \quad \sin \psi_{41} = |v_{41}^{(0)}|.$$

Finally, we obtain a unit vector at the first column by multiplying G_{31} and G_{41} as follows:

$$G_{41} G_{31} G_{21} D_1^H \begin{bmatrix} v_{11}^{(1)} & v_{12}^{(1)} \\ v_{21}^{(1)} & v_{22}^{(1)} \\ v_{31}^{(1)} & v_{32}^{(1)} \\ |v_{41}^{(0)}| & |v_{42}^{(0)}| \end{bmatrix} = \begin{bmatrix} 1 & 0 \\ 0 & v_{22}^{(3)} \\ 0 & v_{32}^{(4)} \\ 0 & v_{42}^{(5)} \end{bmatrix}. \quad (6)$$

We conduct similar procedures on the remaining column sequentially by calculating D_2 , G_{32} , G_{42} , and finally obtain an identity matrix $\mathbf{I}_{M \times N}$.

$$G_{42} G_{32} D_2^H G_{41} G_{31} G_{21} D_1^H \begin{bmatrix} v_{11}^{(1)} & v_{12}^{(1)} \\ v_{21}^{(1)} & v_{22}^{(1)} \\ v_{31}^{(1)} & v_{32}^{(1)} \\ |v_{41}^{(0)}| & |v_{42}^{(0)}| \end{bmatrix} = \begin{bmatrix} 1 & 0 \\ 0 & 1 \\ 0 & 0 \\ 0 & 0 \end{bmatrix}. \quad (7)$$

Setting an original parameter set, i.e., the rotation angles $\{\phi, \psi\}$, exactly reconstructs the original matrix $\hat{\mathbf{V}}$. However, the transmission of the original parameter set still causes a large communication overhead. Therefore, the angle information of ϕ and ψ is quantized before transmission. After the angle information is quantized in some bits, they are serialized across all the subcarriers in a channel and shared between the AP and receiver.

The serialized angles are known as CBR and are contained in IEEE 802.11ac/ax wireless packets. CBR is not broadcasted. Each receiver returns CBR in response to a request sent by the AP it is connected to. If more than one receiver is connected to the AP, the AP sends a request to each receiver in turn to have them return the CBR. Here, approximately 10 to 20 CBR packets are exchanged every second between the AP and wireless devices. These packets normally propagate over the air without encryption, thus a third-party sniffer can easily obtain the CBR binary. It should be noted that the interval is significantly sparse compared to the existing full CSI-based sensing methods, where those that are considered full CSI can be acquired more than 100 times every second. Moreover, CBR is expected to have a smaller amount of information than full CSIs because of some mathematical operations.

CBR is the key element to realizing a wireless sensing system under IEEE 802.11ac/ax standards, although the sparsity, i.e., the smaller amount of information, of CBR makes it challenging to use as an alternative information source to the full CSI. Although we have not yet fully understood the nature of CBRs, we take the first step forward to address the existing challenges.

4. Proposed System: CBR-ACE

4.1 Overview

We design the CBR-ACE system to count human activity that is repeated at a constant interval, by leveraging CBR with IEEE 802.11ac compliant devices. The left side of **Fig. 2** shows the assumed model of our CBR-ACE. We set one Wi-Fi device and one Wi-Fi AP in a room. The CBR-ACE assumes that both the Wi-Fi device and Wi-Fi AP follow the IEEE 802.11ac standard for packet delivery. A sniffer device, i.e., WiPiCap, is connected

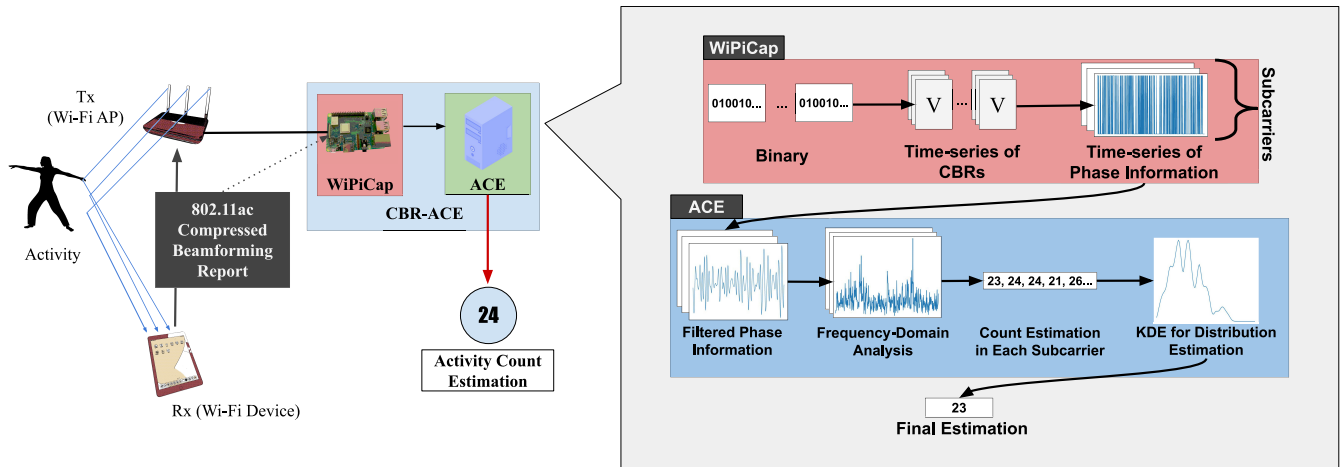


Fig. 2 Overall structure (left) and procedure (right) of our CBR-ACE. CBR-ACE consists of WiPiCap and ACE for human exercise recognition using the CBRs.

to the Wi-Fi AP via a Local Area Network (LAN) cable. WiPiCap continuously sends User Datagram Protocol (UDP) packets to the Wi-Fi device through the Wi-Fi AP to ensure that the Wi-Fi AP repeatedly requests CBR packets to the Wi-Fi device. Meanwhile, WiPiCap captures the CBR packets between the Wi-Fi device and Wi-Fi AP at a rate of approximately 10 Hz. A person repeats an indoor activity at a certain location in the room. CBR-ACE counts the number of indoor repetitive activities using the captured CBR packets.

The right side of Fig. 2 shows the overall procedure of the proposed CBR-ACE, which obtains a time-series of the CBRs for each subcarrier through our WiPiCap. CBR-ACE integrates the following techniques for accurate counts estimation.

- CBR-ACE utilizes the phase information obtained from the time-series of the CBRs for counts estimation.
- ACE adopts the bandpass filter and exponential moving-average (EMA) filter to the raw phase information to eliminate the effect of potential noises.
- CBR-ACE utilizes Kernel Density Estimation (KDE) to determine the estimation result from the results of all the subcarriers.

4.2 WiPiCap: Raspberry Pi-based Packet Sniffer and Binary Decoding

WiPiCap uses a microcomputer, i.e., Raspberry Pi, to realize CBR packet sniffing as well as CBRs reconstruction without the modification of the wireless APs and devices. The source code is available at (<https://github.com/watalabo/WiPiCap>).

To capture CBR packets using the Raspberry Pi, it is necessary to switch its wireless NIC into IEEE 802.11 monitor mode in which all packets (whatever the destination address) are captured by the NIC without an association with the connected AP. However, Raspbian, which is a defacto-standard operating system for the Raspberry Pi hardware, does not provide any means to switch its NIC into the IEEE 802.11 monitor mode. Therefore, WiPiCap utilizes the Nexmon firmware patch [25] for CBR packet capture.

After WiPiCap captures packets between the Wi-Fi AP and Wi-Fi device, it reconstructs the CBRs for each subcarrier, and then reconstructs V matrices described in Section 3. It is worth noting

that V matrices are complex matrices and each element includes amplitude and phase information. In the CBR-ACE, we use the phase information for the count estimation. Time series data of phase are obtained as the same number as that of subcarriers.

4.3 ACE: Signal Processing-based Activity Count Estimation

ACE estimates human activity counts using the phase information of the CBRs and signal processing. Specifically, it performs Fourier transform for the time-series of the phase information, and then estimates the human activity counts from the peak frequency. The proposed ACE does not require training for estimation; hence, it overcomes the computational limitation for the estimation.

ACE first removes noise from the obtained phase information. The noise in the CBR is mainly due to the hardware of the access point or Wi-Fi device and noise from objects other than the motion of the target person. Because the noise caused by the hardware is bursty and of a large amplitude [26], we adopt the EMA filter to eliminate burst noises. The EMA filter has a window size of five packets, i.e., 250 ms, to remove the burst noise, and a band-pass filter to eliminate the frequency components unrelated to the activity. ACE considers the activity interval to be approximately 1 Hz; thus, the band-pass filter [27] passes the frequency components between 0.5 Hz and 1.5 Hz.

If the exercise is repeated at a nearly constant interval, the power of the frequency component corresponding to the interval increases. ACE regards the frequency component with the highest power in each subcarrier as the candidates of the estimated value.

Because each subcarrier experiences a narrowband fading channel based on the activity, it is important to select adequate subcarriers for the count estimation. The existing full CSI-based study selects subcarriers with a larger variance for the recognition [28] because variance is considered to represent the sensitivity of the subcarrier. However, no obvious correlation exists between the recognition accuracy and the variance of the CBRs in each subcarrier from our experiments. Figure 3 shows the relationship between the variance of the subcarrier and the estimated exercise counts for one case. Here, the correct number of the

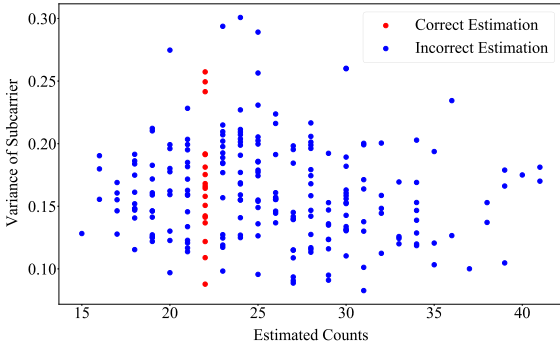


Fig. 3 Example: relationship between subcarrier variance and correct/incorrect estimation results.

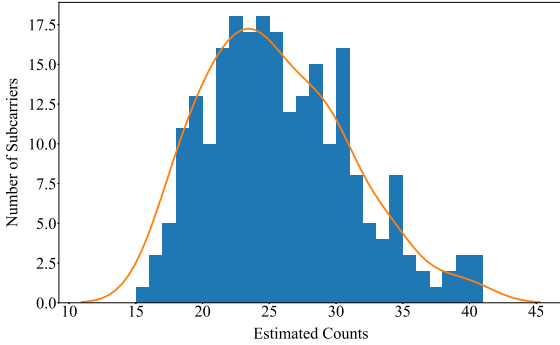


Fig. 4 Example: distribution of estimation values emerged from all subcarriers in a channel. The line in orange color indicates the estimated probability distribution function estimated by KDE.

repetitive activity is 22. Each dot represents one subcarrier, and each subcarrier has a variance and estimated counts. The red dots indicate the adequate subcarriers with no estimation error for the case. It can be observed that a large variance does not necessarily result in a higher estimation accuracy. However, as shown in **Fig. 4**, we also find that the estimates are not completely random, but have a distribution with a peak near the true value.

From those observations, we regard each subcarrier as a *candidate*, and these candidate values emerge from a certain probability distribution function. ACE uses KDE to estimate human exercise counts by utilizing the estimates of all the subcarriers. Particularly, KDE estimates a continuous distribution from the distribution of discrete estimates. Let $x_1, x_2, \dots, x_n \in \mathbb{R}$ be an independent and identically distributed (i.i.d) sample from a distribution F with a density f . The KDE of f , also referred to as the Parzen window estimate, is a nonparametric estimate given by:

$$\hat{f}(x) = \frac{1}{n} \sum_{i=1}^n K_h(x, x_i), \quad (8)$$

where K_h is an arbitrary kernel function with bandwidth h . To ensure $\hat{f}(x)$ is a density, we assume the kernel function satisfies the following conditions:

$$K_h(\cdot, \cdot) \geq 0, \quad \int_{-\infty}^{\infty} K_h(x, \cdot) dx = 1.$$

Our ACE uses the Gaussian function as a kernel function $K_h(x, t)$:

$$K_h(x, x_i) = \frac{1}{\sqrt{2\pi}h} \exp\left(-\frac{\|x - x_i\|^2}{2h^2}\right).$$

Here, the bandwidth of the kernel h has a strong effect on the

estimated density. If h is too small or too large, the estimated density \hat{f} is under or over smoothed. There are some kinds of criterion to determine h , such as the mean integrated square error (MISE) [29], Silverman's rule of thumb [30], and Scott's rule of thumb [31]. Because purpose of using KDE in the proposed ACE is to determine the best estimate from the estimated density, h is a particularly important factor to ensure the accuracy of the estimation. We adopt a grid search method to determine the optimum h . Specifically, we carry out KDE with the different bandwidths from 1 to 10 in 0.1 intervals and adopt the best bandwidth that minimizes the error between the estimated density and the original discrete density.

From the process described above, ACE calculates the cumulative distribution function (CDF) of the estimated density and regards the fifty percentile point as the final estimated counts. In our observation, the fifty percentile point is a better indicator than the simple median, average, and density peak.

5. Experiments

5.1 Experimental Settings

Implementation: We implemented CBR-ACE on COTS wireless devices. We used TP-Link Archer C6 as the Wi-Fi AP, and MacBook Pro (2020), iPad (5th Generation), and Galaxy Note 10 Lite as the Wi-Fi devices. We installed WiPiCap on the Raspberry Pi 3 Model B+ with a BCM434355c0 chip. Experiments were performed in the 5 GHz frequency band with a channel bandwidth of 80 MHz. Note that our system can work with IEEE 802.11ax utilizing CBR as well as IEEE 802.11ac. Moreover, in this experiment, only one device is connected to the AP at a time, but our system can work with multiple devices connected to the AP at the same time. During the experiments, the average reception rate of CBR packets was 9.7 Hz. Here, the packet sampling interval is non-uniform owing to the interference caused by other Wi-Fi devices in the same channel. We used linear interpolation for the uniform sampling interval. Additionally, the sampling interval was still sufficient enough for the count estimation because the activity interval was approximately 1 Hz.

Experiment Environment: **Figure 5** shows the experiment environment. The experiment was carried out in a general office room. One subject stands at either place 1 (P1) or place 2 (P2) in **Fig. 5**, and exercises at that place for 30 s. P1 is on the line connecting the positions of the Wi-Fi AP and Wi-Fi device, whereas P2 is outside the line. The experiments were conducted 890 times for the same subject from October 12, 2020 to October 30, 2020.

Target Activities: **Figure 5** shows the target of the three activities in our experiments: swing, step, and twist. The swing is arm swinging, the step is a stepping motion, and the twist keeps the subject's pelvis stable as the subject rotates the rib cage right and left. In each experiment, we estimate the number of repetitions for each activity within 30 s.

Metric: The mean absolute error (MAE) was applied between the ground-truth number of the repetitions and the estimated number of the repetition as the recognition accuracy.

5.2 Effect of Filters and KDE

Our ACE assumes an EMA filter and a bandpass filter, and

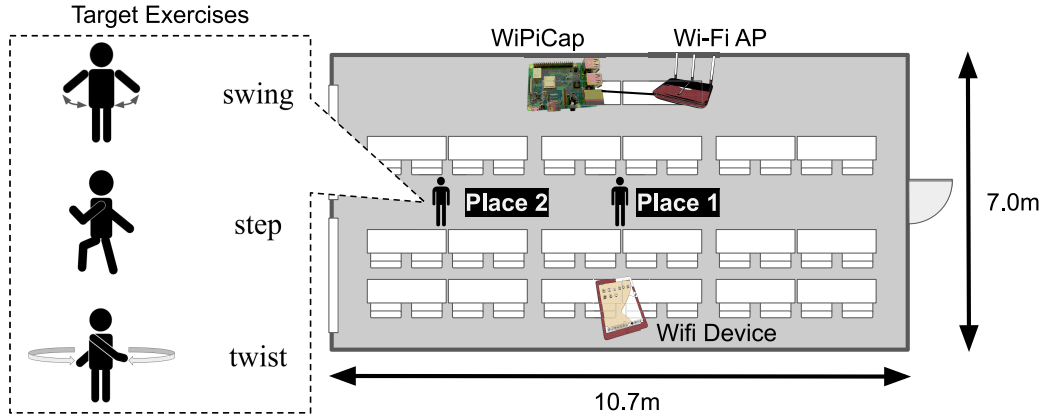


Fig. 5 Experiment environment. We set one Wi-Fi AP and one Wi-Fi device in a room, and one subject repeats a target exercise at place 1 or place 2 for 30 s.

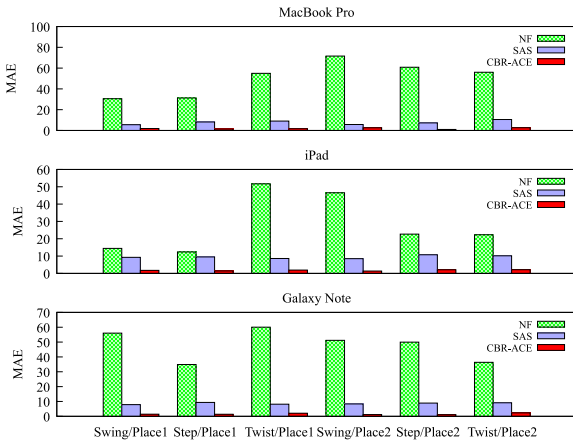


Fig. 6 Accuracy improvement with filters and KDE: our filters and KDE are effective compared with NF and SAS.

then estimates an optimal value using KDE. To clarify their significance in the estimation, we first evaluated the estimation accuracy with/without the filters and KDE. **Figure 6** shows the MAE of the comparative methods for each activity using the different Wi-Fi devices. Here, we used two comparative schemes: no filters (NF) and filters with the averaged estimated results across all subcarriers (SAS). When no filter is applied, the average error is 42.43 times. When the filter is applied and the estimates for all subcarriers are simply averaged, an average error of 8.6 times is achieved. On the other hand, the estimation using CBR-ACE achieves an average error of 1.73 times. Clearly, both the filters and KDE yield better estimation accuracy irrespective of the activities and Wi-Fi devices.

5.3 Effect of Criteria for Count Estimation

We demonstrated that our filters and KDE method realized accurate count estimation using the CBRs. Thereafter, we discussed the effect of the criteria for the final count decision on the estimation accuracy. We prepared a comparative method (VAR) inspired by Ref. [28] and implemented the comparative method using the second highest variance subcarriers for estimation. To unify other conditions with our CBR-ACE, the filters and their parameters applied to the time-series of the phase information are the same as those of the proposed CBR-ACE.

Figure 7 shows the MAE of the proposed CBR-ACE and

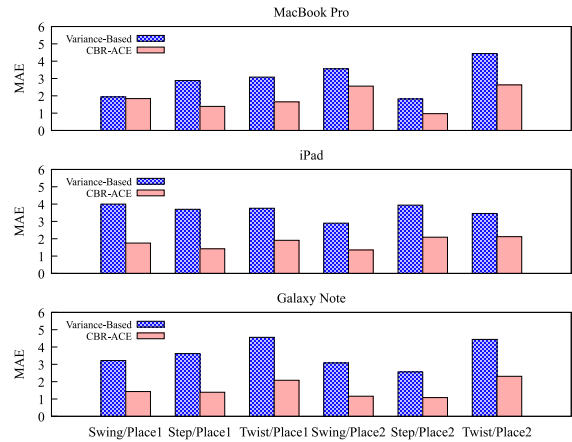


Fig. 7 Comparison between the variance based method and proposed CBR-ACE.

variance-based method [28] for each exercise using the different Wi-Fi devices. From the figure, the following observations are made.

- CBR-ACE overwhelms the variance-based method for all cases.
- A relationship exists between the kind of activities and recognition accuracy. For example, because of the difference of degree of freedom, the twist has a lower estimation accuracy, whereas the step has a higher one.
- CBR-ACE achieves almost the same estimation accuracy regardless of the location and Wi-Fi devices.

For example, our CBR-ACE achieves the best MAE of 0.97, and the worst MAEs of 2.09 and 2.63 at places 1 and 2, respectively. However, the variance-based method achieves the best MAE of 1.94, and the worst MAEs of 4.56 and 4.44 at places 1 and 2, respectively.

5.4 Micro-benchmark: Effect of KDE with Small Number of Samples

With a larger number of subcarriers, the distribution estimated by KDE becomes closer to the original discrete distribution, and similar results can be obtained using either the median of the discrete distribution or that of the estimated distribution. However, with a limited number of subcarriers, it is expected that KDE is more effective determining the optimal estimate, i.e., narrow

Table 2 Micro Benchmark: KDE has an advantage in terms of the estimation accuracy with a smaller number of samples.

Number of samples	Criteria	MAE	Standard Deviation
10	KDE	2.38	1.79
	Median	3.03	2.37
20	KDE	2.04	1.58
	Median	2.80	2.34

Table 3 MAE performance using the 40th, 50th, and 60th percentile points of the estimated density.

Device	k -th point	MAE	Standard Deviation
MacBook Pro	40%	1.99	3.09
	50%	1.95	2.16
	60%	2.36	2.39
iPad	40%	2.43	3.89
	50%	1.78	2.18
	60%	1.76	1.72
Galaxy Note	40%	2.09	2.98
	50%	1.58	1.62
	60%	1.81	1.99

Table 4 Average CBRs acquisition per second for each device.

Device	MacBook Pro	iPad	Galaxy Note
Place 1	10.03	11.00	9.73
Place 2	10.13	8.03	9.60

channel bandwidth such as 20 MHz and 40 MHz.

To verify the effectiveness of KDE with a limited number of samples, we carried out an estimation with the limited number of subcarriers. For this benchmark, we select 300 cases from the experimental data, randomly extract 10 and 20 subcarriers from 234 subcarriers included in the 80 MHz channel, and estimate the density with ACE. In **Table 2**, we compare the estimation accuracy using the KDE and median of the samples with the limited number of samples. KDE yields better estimation accuracy in terms of the MAE and standard deviation compared with the median-based method.

5.5 Effect of k -th Percentile Point on Estimation Accuracy

The proposed ACE used the 50th percentile point of the estimated density obtained from the KDE for the activity estimation. This section discusses the effect of the selected percentile points, i.e., 40th, 50th, and 60th, on the estimation accuracy. Here, we compared the MAE and the corresponding standard deviation for each device across all places and activities.

Table 3 presents the effect of the selected percentile points on the MAE and standard deviation. The bold ones indicate the best MAE for each device. It can be observed that the 50th percentile point achieves the best MAE except for the iPad.

Here, we discuss why the 50th percentile point was not optimal for the iPad in terms of the CBR acquisition rate. **Table 4** lists the average acquisition rate of the CBR packets in each place and device. At place 2, it can be observed that the average acquisition rate of the iPad is lower than that of the other devices. In this case, the proposed CBR-ACE interpolates the CBR packets to be distributed evenly in time. However, the interpolation may cause a smaller estimated number of repetitions compared with the ground-truth number of repetitions, resulting in a larger MAE at the 50th percentile point.

6. Conclusion and Future Work

We proposed a novel wireless sensing system, CBR-ACE, for human activity count estimation. To the best of our knowledge, CBR-ACE is the first wireless sensing system to recognize human activity counts using the CBRs. The advantage of the CBR-based system is that it accepts COTS wireless devices, which are compliant with IEEE 802.11ac and 11ax, with no strict hardware and software requirements. The experiments show that our CBR-ACE can realize accurate activity count estimation using filters and KDE for the measured CBRs.

Future work includes improving the accuracy of CBR-ACE by combining with machine learning methods. Furthermore, we plan to acquire CBRs under various environments to discuss the versatility of our CBR-ACE.

Acknowledgments This work was supported in part by the Japan Society for the Promotion of Science (JSPS) KAKENHI under Grant JP19H01101, in part by the JST PRESTO, Japan, under Grant JPMJPR2032, and in part by Nippon Telegraph and Telephone Corporation Access Network Service Systems Laboratories.

References

- [1] Brynjolfsson, E., Horton, J.J., Ozimek, A., Rock, D., Sharma, G. and TuYe, H.: COVID-19 and Remote Work: An Early Look At Us Data, *National Bureau of Economic Research*, No.27344, pp.1–26 (2020).
- [2] Ayhan, B., Kwan, C., Budavari, B., Larkin, J., Gribben, D. and Li, B.: Video Activity Recognition With Varying Rhythms, *IEEE Access*, Vol.8, pp.191997–192008 (2020).
- [3] Dyo, V., Ellwood, S.A., MacDonald, D.W., Markham, A., Mascolo, C., Pásztor, B., Scellato, S., Trigoni, N., Wohlers, R. and Yousef, K.: Evolution and sustainability of a wildlife monitoring sensor network, *ACM SenSys*, pp.127–140 (2010).
- [4] Grzeszick, R., Lenk, J.M., Rueda, F.M., Fink, G.A., Feldhorst, S. and ten Hompel, M.: Deep Neural Network based Human Activity Recognition for the Order Picking Process, *Proc. 4th International Workshop on Sensor-based Activity Recognition and Interaction, iWOAR '17*, No.Article 14, pp.1–6, Association for Computing Machinery (2017).
- [5] Jiang, W. and Yin, Z.: Human Activity Recognition Using Wearable Sensors by Deep Convolutional Neural Networks, *Proc. 23rd ACM International Conference on Multimedia, MM '15*, pp.1307–1310, Association for Computing Machinery (2015).
- [6] Sharma, S., Mohammadmoradi, H., Heydariaan, M. and Gnawali, O.: Device-Free Activity Recognition Using Ultra-Wideband Radios, *2019 International Conference on Computing, Networking and Communications (ICNC)*, pp.1029–1033 (2019).
- [7] Wang, W., Liu, A.X., Shahzad, M., Ling, K. and Lu, S.: Device-Free Human Activity Recognition Using Commercial WiFi Devices, *IEEE Journal on Selected Areas in Communications*, Vol.35, No.5, pp.1118–1131 (2017).
- [8] Ding, S., Chen, Z., Zheng, T. and Luo, J.: RF-net: A unified meta-learning framework for RF-enable one-shot human activity recognition, *Proc. 18th Conference on Embedded Networked Sensor Systems*, pp.517–530, ACM (2020).
- [9] Huang, M., Liu, J., Gu, Y., Zhang, Y., Ren, F., Wang, X. and Li, J.: Your WiFi Knows You Fall: A Channel Data-Driven Device-Free Fall Sensing System *ICC 2019*, pp.1–6 (2019).
- [10] Li, F., Valero, M., Shahriar, H., Khan, R.A. and Ahamed, S.I.: Wi-COVID: A COVID-19 Symptom Detection and Patient Monitoring Framework using WiFi, *Smart Health*, Vol.19, pp.1–17 (2021).
- [11] Huang, W., Liu, Y., Zhu, S., Wang, S. and Zhang, Y.: TSCNN: A 3D Convolutional Activity Recognition Network Based on RFID RSSI, *2020 International Joint Conference on Neural Networks (IJCNN)*, pp.1–8 (2020).
- [12] Yao, L., Sheng, Q.Z., Li, X., Gu, T., Tan, M., Wang, X., Wang, S. and enjie Ruan: Compressive Representation for Device-Free Activity Recognition with Passive RFID Signal Strength, *IEEE Trans. Mob. Comput.*, Vol.17, No.2, pp.293–306 (2018).
- [13] Kim, Y. and Ling, H.: Human Activity Classification Based on Micro-Doppler Signatures Using a Support Vector Machine, *IEEE Trans.*

- Geosci. Remote Sens.*, Vol.47, No.5, pp.1328–1337 (2009).
- [14] Piriyaikitakonkij, M., Warin, P., Lakhon, P., Leelaarporn, P., Kumchaisemak, N., Suwajanakorn, S., Pianpanit, T., Niparnan, N., Mukhopadhyay, S.C. and Wilaiprasitporn, T.: SleepPoseNet: Multi-View Learning for Sleep Postural Transition Recognition Using UWB, *IEEE J Biomed Health Inform.*, Vol.25, No.4, pp.1305–1314 (2021).
- [15] Adib, F., Kabelac, Z., Katabi, D. and Miller, R.C.: 3D tracking via body radio reflections, *11th USENIX Symposium on Networked Systems Design and Implementation (NSDI 14)*, pp.317–329 (2014).
- [16] Ma, Y., Arshad, S., Muniraju, S., Torkildson, E., Rantala, E., Doppler, K. and Zhou, G.: Location- and Person-Independent Activity Recognition with WiFi, Deep Neural Networks, and Reinforcement Learning, *ACM Trans. Internet Things*, Vol.2, No.1, pp.1–25 (2021).
- [17] Wang, W., Liu, A.X., Shahzad, M., Ling, K. and Lu, S.: Understanding and Modeling of WiFi Signal Based Human Activity Recognition, *Proc. 21st Annual International Conference on Mobile Computing and Networking, MobiCom '15*, pp.65–76, Association for Computing Machinery (2015).
- [18] Halperin, D., Hu, W., Sheth, A. and Wetherall, D.: Tool release: gathering 802.11n traces with channel state information, *SIGCOMM Comput. Commun. Rev.*, Vol.41, No.1, p.53 (2011).
- [19] Xie, Y., Li, Z. and Li, M.: Precise Power Delay Profiling with Commodity Wi-Fi, *IEEE Trans. Mob. Comput.*, Vol.18, No.6, pp.1342–1355 (2019).
- [20] Suraweera, N., Winter, A., Sorensen, J., Li, S., Johnson, M., Collings, I.B., Hanly, S.V., Ni, W. and Hedley, M.: Passive Through-Wall Counting of People Walking Using WiFi Beamforming Reports, *IEEE Syst. J.*, pp.1–7 (2020).
- [21] Miyazaki, M., Ishida, S., Fukuda, A., Murakami, T. and Otsuki, S.: Initial Attempt on Outdoor Human Detection using IEEE 802.11ac WLAN Signal, *2019 IEEE Sensors Applications Symposium (SAS)*, pp.1–6 (2019).
- [22] Kato, S., Fukushima, T., Murakami, T., Abeyskera, H., Iwasaki, Y., Fujihashi, T., Watanabe, T. and Saruwatari, S.: CSI2Image: Image Reconstruction From Channel State Information Using Generative Adversarial Networks, *IEEE Access*, Vol.9, pp.47154–47168 (2021).
- [23] Ueng, F.B., Wang, H.F., Chang, R. and Jeng, L.D.: Zero Forcing and Minimum Mean Square Error Equalization for OFDM-CDMA Multiuser Detection in Multipath Fading Channels (2006).
- [24] IEEE Computer Society: Part 11: Wireless Lan Medium Access Control (MAC) and Physical Layer (PHY) Specifications, IEEE Std 802.11-2007, Vol.2007, No.6 (2007).
- [25] Schulz, M., Wegemer, D. and Hollick, M.: Nexmon: The C-based Firmware Patching Framework (2017).
- [26] Zhang, T., Song, T., Chen, D., Zhang, T. and Zhuang, J.: WiGrus: A Wi-Fi-Based Gesture Recognition System Using Software-Defined Radio, *IEEE Access*, Vol.7, pp.131102–131113 (2019).
- [27] Guo, X., Liu, B., Shi, C., Liu, H., Chen, Y. and Chuah, M.C.: WiFi-Enabled Smart Human Dynamics Monitoring (2017).
- [28] Wang, X., Yang, C. and Mao, S.: PhaseBeat: Exploiting CSI Phase Data for Vital Sign Monitoring with Commodity WiFi Devices, *2017 IEEE 37th International Conference on Distributed Computing Systems (ICDCS)*, pp.1230–1239 (2017).
- [29] Park, B.U. and Marron, J.S.: Comparison of Data-Driven Bandwidth Selectors, *Journal of the American Statistical Association*, Vol.85, No.409, pp.66–72 (1990).
- [30] Silverman, B.W.: *Density estimation for statistics and data analysis*, Vol.26, CRC press (1986).
- [31] Terrell, G.R. and Scott, D.W.: Oversmoothed Nonparametric Density Estimates, *Journal of the American Statistical Association*, Vol.80, No.389, pp.209–214 (1985).



Sorachi Kato received his B.E. from Osaka University in 2021. He is currently a student at the Graduate School of Information Science and Technology, Osaka University. His research interests include wireless sensing and MIMO communication. He is a student member of IPSJ and IEEE.



Tomoki Murakami received his B.E., M.E., and Dr. Eng. degrees from Waseda University, Japan in 2006, 2008, and 2015, respectively. In 2008, he joined the NTT Network innovation Laboratories, Nippon Telegraph and Telephone Corporation (NTT), Yokosuka, Japan. He is currently a Research Engineer in the Wireless

Access Systems Project. His current research interests are high efficiency technologies for future wireless systems. He received the Young Engineer Award from the IEICE in 2010, the Active Research Award from IEICE AP (Antenna and Propagation) in 2010, the Best Tutorial Paper Award from IEICE Communications society in 2014, the Best Paper Award and the KIYASU-Zen'iti Award from the IEICE in 2015, and the Best Paper Award from IEICE on AP in 2016. He is a member of IEEE and IEICE.



Takuya Fujihashi received his B.E. degree in 2012 and M.S. degree in 2013 from Shizuoka University, Japan. In 2016, he received his Ph.D. degree from the Graduate School of Information Science and Technology, Osaka University, Japan. He has been an assistant professor at the Graduate School of Information Science

and Technology, Osaka University since April, 2019. His research interests are in the area of video compression and communications, with a focus on immersive video coding and streaming.



Takashi Watanabe is a Professor of the Graduate School of Information Science and Technology, Osaka University, Japan. He received his B.E., M.E. and Ph.D. degrees from Osaka University, Japan, in 1982, 1984 and 1987, respectively. He joined the Faculty of Engineering, Tokushima University as an assistant professor

in 1987 and moved to the Faculty of Engineering, Shizuoka University in 1990. He was a visiting researcher at University of California, Irvine from 1995 through 1996. He has served on the many program committees for networking conferences: IEEE, ACM, IPSJ, IEICE (The Institute of Electronics, Information and Communication Engineers, Japan).



Shunsuke Saruwatari received his Dr. Sci. degree from the University of Tokyo in 2007. From 2007 to 2008, he was a visiting researcher at the Illinois Genetic Algorithm Laboratory, University of Illinois at Urbana-Champaign. From 2008 to 2012, he was a research associate at the RCAST, the University of Tokyo. From

2012 to 2016, he was an assistant professor at Shizuoka University. He has been an associate professor at Osaka University since 2016. His research interests are in the areas of wireless networks, sensor networks, and system software.